Science Translational Medicine AAAS

Indocyanine Green Enables Near-Infrared Fluorescence Imaging of Lipid-Rich, Inflamed Atherosclerotic Plaques

Claudio Vinegoni, *et al.*

Sci Transl Med **3**, 84ra45 (2011);
DOI: 10.1126/scitranslmed.3001577

Editor's Summary

Greenify Your Arteries

Many have taken it upon themselves to go green, perhaps by turning down the thermostat, swapping out old light bulbs, or even buying a hybrid car. But who would have thought that even your heart doctor can take part in this green initiative? As described by Vinegoni et al., going green may be just what you and your arteries need to detect atherosclerotic plaques residing within them.

Indocyanine green (ICG) is a Food and Drug Administration approved dye for imaging the vascular system at near-infrared (NIR) wavelengths (~800 nm) wavelengths that boast limited photon absorption by blood and low tissue autofluorescence. ICG is also quickly absorbed by lipid-rich plaques and cells, making it a potentially useful plaque-imaging agent. Vinegoni and colleagues decided to test this hypothesis in rabbit models of atherosclerosis. Lipid-rich, inflamed atheromas were induced in 19 cholesterol-fed rabbits with balloon injury of the aorta. Eight weeks after injury, rabbits received an injection of ICG. Only 45 min later, the animals were killed for fluorescence imaging, which showed strong focal signals in the abdominal aorta and iliac arteries areas that colocalized with atherosclerotic plaques. Conversely, control animals showed minimal NIR fluorescence signal.

The authors then performed in vivo NIR fluorescence imaging of ICG in live animals. Using a clinical-type intravascular guidewire and a previously described pullback technique, they were able to sense atheroma in the coronary arteries of five rabbits. The location of these plaques was confirmed by x-ray angiography and intravascular ultrasound. Furthermore, ICG localization to human atheroma was confirmed ex vivo with freshly resected carotid endarterectomy specimens from four patients. Together, these animal and human data suggest direct translation to the clinic and highlight the potential application of ICG as a routine, green screening tool for atherosclerosis.

Science Translational Medicine (print ISSN 1946-6234; online ISSN 1946-6242) is published weekly, except the last week in December, by the American Association for the Advancement of Science, 1200 New York Avenue NW, Washington, DC 20005.

ATHEROSCLEROSIS

Indocyanine Green Enables Near-Infrared Fluorescence Imaging of Lipid-Rich, Inflamed Atherosclerotic Plaques

Claudio Vinegoni,[1,2] Ion Botnaru,[3] Elena Aikawa,[1,4] Marcella A. Calfon,[3] Yoshiko Iwamoto,[2] Eduardo J. Folco,[4] Vasilis Ntziachristos,[5] Ralph Weissleder,[1,2] Peter Libby,[4] Farouc A. Jaffer[1,3]*

New high-resolution molecular and structural imaging strategies are needed to visualize high-risk plaques that are likely to cause acute myocardial infarction, because current diagnostic methods do not reliably identify at-risk subjects. Although molecular imaging agents are available for low-resolution detection of atherosclerosis in large arteries, a lack of imaging agents coupled to high-resolution modalities has limited molecular imaging of atherosclerosis in the smaller coronary arteries. Here, we have demonstrated that indocyanine green (ICG), a Food and Drug Administration–approved near-infrared fluorescence (NIRF)–emitting compound, targets atheromas within 20 min of injection and provides sufficient signal enhancement for in vivo detection of lipid-rich, inflamed, coronary-sized plaques in atherosclerotic rabbits. In vivo NIRF sensing was achieved with an intravascular wire in the aorta, a vessel of comparable caliber to human coronary arteries. Ex vivo fluorescence reflectance imaging showed high plaque target-to-background ratios in atheroma-bearing rabbits injected with ICG compared to atheroma-bearing rabbits injected with saline. In vitro studies using human macrophages established that ICG preferentially targets lipid-loaded macrophages. In an early clinical study of human atheroma specimens from four patients, we found that ICG colocalized with plaque macrophages and lipids. The atheroma-targeting capability of ICG has the potential to accelerate the clinical development of NIRF molecular imaging of high-risk plaques in humans.

INTRODUCTION

Rupture of atherosclerotic plaques and its associated thrombotic complications of myocardial infarction, stroke, and ischemic limbs remain leading causes of morbidity and mortality worldwide. Although various invasive and noninvasive imaging techniques can interrogate structural and compositional aspects of atheroma, only recently have molecular imaging strategies, such as nanoparticle-enhanced magnetic resonance imaging and fluorine-18-fluorodeoxyglucose positron emission tomography, enabled the in vivo detection of high-risk plaque features, such as inflammation, in patients (*1*, *2*). Although molecular imaging of larger arterial beds, such as the aorta, carotid, and iliac arteries, has experienced rapid clinical translation, high-resolution molecular imaging studies of smaller coronary arterial plaques remain scarce. Two main features contribute to this shortfall: (i) the requirement for high spatiotemporal resolution to image small-volume coronary atheroma, which can be less than 0.1 ml (*3*) and which typically necessitates intravascular imaging approaches (*4*), and (ii) the lack of sensitive molecular imaging agents that can be coupled to high-resolution detection modalities.

To address the first limitation, we recently developed high-resolution near-infrared fluorescence (NIRF) molecular imaging technology to sense protease activity in atheroma (*5*). This approach validated a clinical-type coronary artery guidewire for sensing intravascular NIRF signals at high resolution, and capitalized on the favorable optical properties of the near-infrared (NIR) window, namely, relatively limited photon absorption by blood and reduced tissue autofluorescence (*6*, *7*). Although the intravascular NIRF guidewire addressed a device-based need for high-resolution coronary arterial molecular imaging, the lack of a clinical NIRF molecular imaging agent has remained a barrier to translation. We therefore reviewed potential clinical candidate agents and recognized that indocyanine green (ICG; $C_{43}H_{47}N_2O_6S_2Na$, 775 daltons), an amphiphilic NIR fluorochrome, appeared promising for molecular imaging of atherosclerosis in the clinic. ICG is a clinical cardiac and hepatic blood flow reporter that has been used for more than 5 decades (*8*, *9*), and is approved by the Food and Drug Administration (FDA) for NIRF imaging of retinal and choroidal vasculature since the 1970s (*10*–*12*). ICG comprises two lipophilic polycyclic moieties (benzoindotricarbocyanin) linked by a polymethine chain. A sulfonate group is bound to each polycyclic part, enhancing water solubility and conferring amphiphilic properties. As a result, after injection, ICG binds rapidly to plasma proteins, primarily albumin. ICG absorption maximum is 785 nm in aqueous solution, and red shifts to 805 nm in blood, whereas its fluorescence emission maximum is 815 nm in aqueous solution, shifting to 830 nm in blood. After injection, ICG is rapidly taken up by the liver and then excreted, unchanged, into the bile, with an elimination half-life of 2 to 4 min in subjects with normal liver function (*10*).

ICG may detect certain molecular and cellular targets relevant to atherosclerosis; for example, ICG binds low-density lipoprotein (LDL) and high-density lipoprotein (HDL), consistent with its lipophilic properties (*13*). Moreover, ICG can illuminate local inflammation in diseases of the eye (*10*, *14*) and of the joints (*15*). On the basis of its high-resolution NIRF imaging capabilities, its lipophilic properties, and its predilection to accumulate at sites of inflammation, we hypothesized that ICG would enable in vivo detection of lipid-rich, inflamed atheroma and sought to test this hypothesis in a rabbit model of atherosclerosis. We also examined the ability of ICG to target human macrophages and human atherosclerosis specimens ex vivo.

[1]Center for Molecular Imaging Research, Massachusetts General Hospital, Boston, MA 02114, USA. [2]Center for Systems Biology, Massachusetts General Hospital, Boston, MA 02114, USA. [3]Cardiovascular Research Center and Cardiology Division, Massachusetts General Hospital, Boston, MA 02114, USA. [4]Cardiovascular Division, Brigham and Women's Hospital, Boston, MA 02114, USA. [5]Institute for Biological and Medical Imaging, Helmholtz Zentrum München und Technische Universität München, Munich 80333, Germany.
*To whom correspondence should be addressed. E-mail: fjaffer@mgh.harvard.edu

RESULTS

ICG rapidly targets atherosclerosis on ex vivo NIRF imaging

To explore whether ICG could rapidly target experimental atherosclerosis, we generated lipid-rich, inflammatory atheroma in cholesterol-fed New Zealand white rabbits (n = 19 total) (*16*, *17*) with balloon injury of the aorta. Eight weeks after balloon injury, rabbits received an injection of ICG (n = 17) at 1.5 mg/kg intravenous bolus, which is an FDA-approved dose for clinical ICG applications (*18*), or saline (n = 2). An additional two normal rabbits (chow diet, not balloon-injured) were also injected with ICG (1.5 mg/kg) and served as controls. Forty-five minutes after ICG or saline injection, rabbits were killed and imaged with fluorescence reflectance imaging (FRI). The plaque signal-to-noise ratio (SNR) and the plaque target-to-background ratio (TBR) were calculated for the acquired NIRF images. In atheroma-bearing animals injected with ICG, we used ex vivo macroscopic FRI to note a strong focal NIRF signal in the abdominal aorta and iliac arteries (Fig. 1A). These areas colocalized with atherosclerotic plaques, as detected by white light (WL) images. The vessel SNR was 13.9 ± 7.5 in this group. Control animals exhibited very low (170 to 630% reduced) NIRF signals (Fig. 1, B and C), with a vessel SNR of 1.9 ± 0.1 in the atheroma/saline-injected group and 5.2 ± 0.1 in the normal/ICG-injected group (P < 0.05) (Fig. 1D). In rabbits with atheroma, the peak plaque TBR in the ICG-injected group was more than 110% higher than in the saline group (P < 0.05) (Fig. 1E).

ICG colocalizes with lipid- and macrophage-rich atheroma

Fluorescence microscopy and histological analysis revealed that ICG plaque fluorescence colocalized with neutral lipid (for example, triglyceride)–rich areas in rabbit atheroma, as visualized by Oil red O (ORO) staining (Fig. 2, A and B). Areas of intense ORO and ICG staining were noted deep within the intimal plaque and often near the border with the external elastic lamina (Fig. 2, A.1 and B). The ICG signal appeared strongest in ORO-stained zones with dense areas of lipid, rather than the smaller, punctate ORO-positive zones. ICG also colocalized with a subset of RAM-11–positive plaque macrophages, particularly lipid-associated foam cells, as evidenced by ORO staining (Fig. 2, A.2 and B). In rabbits, the association of ICG with other plaque macrophages appeared less robust, because some RAM-11–positive areas did not reveal ICG fluorescence (Fig. 2, A.2 and B). ICG also deposited far less in intimal areas containing smooth muscle cells (Fig. 2A.3), endothelial cells (Fig. 2A.4), collagen (Fig. 2A.5), or elastin (Fig. 2A.6).

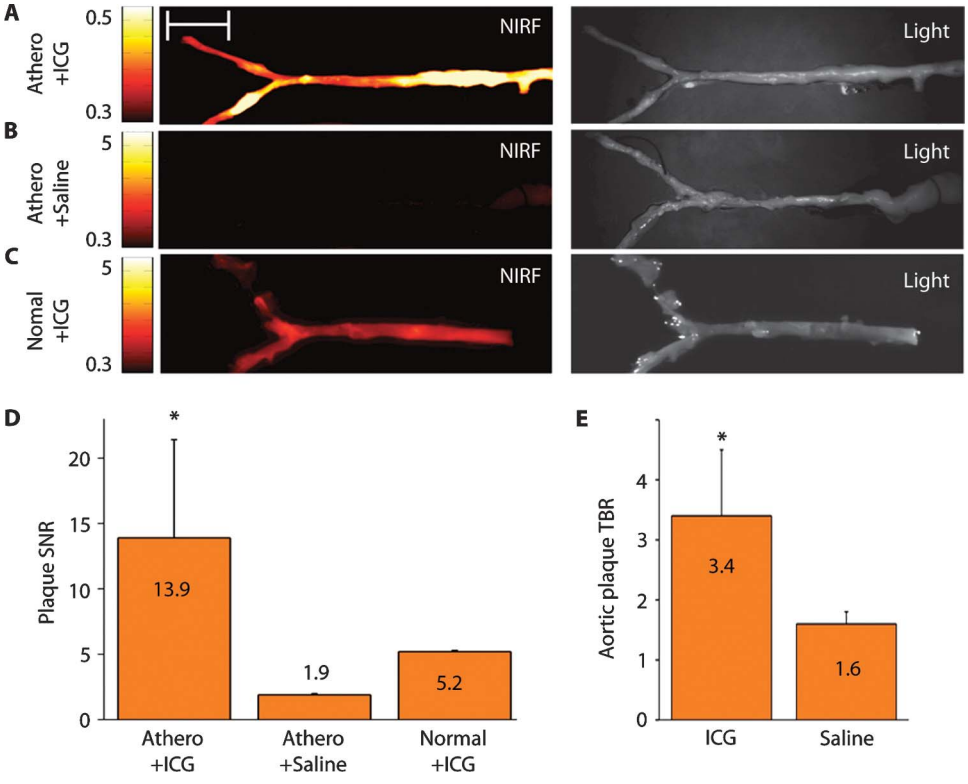

Fig. 1. ICG rapidly targets atheroma in rabbit arteries and provides NIRF signal enhancement. Atheroma-bearing or normal rabbits were injected with either ICG or saline and then killed after 45 min. (**A** to **C**) Ex vivo fluorescence reflectance images (FRI) of aortas obtained at 800 nm (left column; fire color lookup table) and their corresponding white light images (right column). Scale bar, 2 cm. (A) A strong focal arterial NIRF signal colocalizes with atherosclerotic plaques seen in the white light image of atheroma-bearing animals. (B) The saline-injected, atheroma-bearing group shows minimal NIRF arterial signal. (C) Normal, uninjured rabbits injected with ICG generated reduced, diffused NIRF signals. (**D**) Signal-to-noise ratios (SNRs) were calculated for ICG-injected, atheroma-bearing animals (n = 17); saline-injected, atheroma-bearing animals (n = 2); and ICG-injected normal animals (n = 2). The SNR in atheroma-bearing, ICG-injected animals was significantly higher than in control groups (*P < 0.05, one-way ANOVA test across all three groups). (**E**) Plaque target-to-background ratios (TBRs) were significantly higher than those of the saline control group (*P < 0.05, unpaired t test). Data are reported as mean ± SD.

ICG generates plaque NIR fluorescence and is distinct from autofluorescence

Multichannel fluorescence microscopy was used to assess the specificity of ICG for plaque targeting. ICG fluorescence (845 nm) colocalized with ORO-positive areas (Fig. 3, A and B), whereas the autofluorescence signal (535 nm) emanated from elastin fibers in the tunica media (Fig. 3, A to C). Atheroma sections from saline-injected rabbits demonstrated relatively little NIR fluorescence but still showed autofluorescence signals from the media (Fig. 3C).

Comparison of the atheroma-targeting profile of ICG with a vascular permeability agent

We noted mild superficial ICG enhancement of the luminal border infrequently in some atheromatous areas (Fig. 3, A and B) and occasionally even in ORO-negative areas, without evidence of atherosclerosis (Fig. 3B). Therefore, to examine whether heightened endothelial permeability from atherosclerosis and/or a hyperlipidemic milieu accounted for ICG deposition in

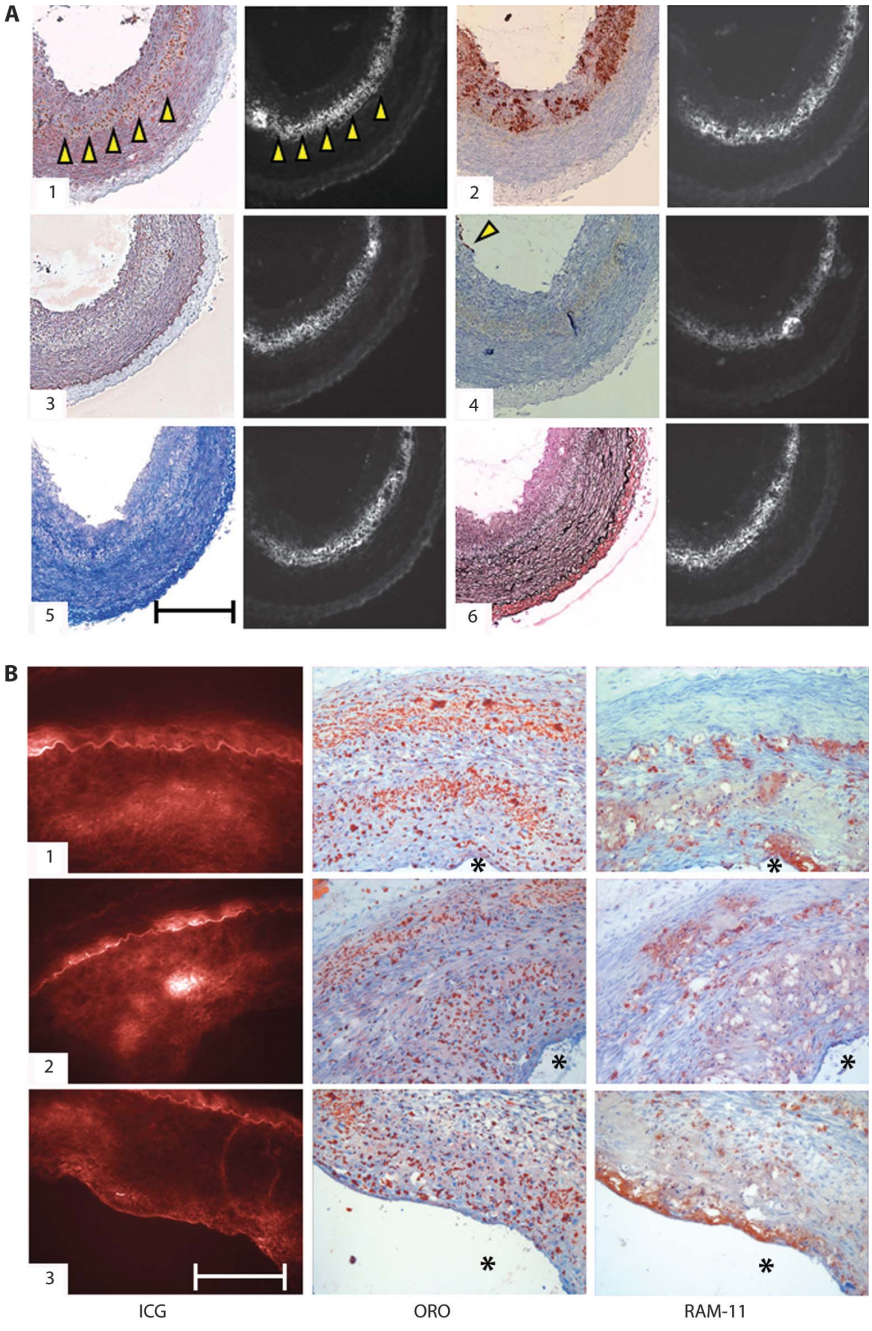

Fig. 2. Histological assessment of ICG targeting of rabbit atheroma. (**A**) Correlative light microscopy and fluorescence microscopy of ICG deposition in atherosclerosis reveal ICG colocalization with lipid-rich and macrophage-abundant areas of atheroma sections. (1) Oil red O (ORO) stain of neutral lipid shows colocalization with ICG signal. Arrowheads highlight the lipid-rich zone. (2) RAM-11–positive macrophages (dark brown stain) colocalize with ICG, particularly in dense, lipid-associated areas. (3) Immunoreactive smooth muscle cells (α-actin; brown stain) minimally colocalize with the matched ICG fluorescent area. (4) A few endothelial cells ($CD31^+$) are present at the luminal surface (arrowhead). Collagen (5) (stained blue with Masson's trichrome) and elastin fibers (6) (stained black with van Gieson's stain) show very little colocalization with ICG. All histological slices are adjacent (6 μm). Fluorescence microscopic images of ICG distribution (854 nm) in all sections were obtained for each slice before staining. Scale bar, 200 μm. (**B**) Histopathological and fluorescence microscopic deposition of ICG in atheroma sections from three different animals (one to three). From left to right: ICG fluorescence (845 nm; false-colored red), ORO staining of neutral lipid, and RAM-11–positive macrophages. Within each group, all images are from adjacent sections (6 μm). Asterisks denote lumen. Scale bar, 100 μm.

arteries, Evans blue, a chemical agent that reveals vascular permeability, and ICG were co-injected into atheroma-bearing rabbits (n = 3). Rabbits were then killed 45 min later. Capitalizing on the known profile of Evans blue in atherosclerosis (*19*) and its fluorescence properties [excitation range, 400 to 630 nm; maximum peak emission, 660 nm (*20*)], we performed multichannel fluorescence microscopy on atheromas that were resected from the animals. Imaging at 710 nm, we could see that Evans blue deposited homogeneously within the plaque, indicating impaired endothelial barrier function (*19*, *21*) (Fig. 4A). In contrast, ICG localized in more restricted regions within the atherosclerotic intima (Fig. 4B), as demonstrated above (Figs. 2 and 3).

ICG binds acetylated LDL and albumin and internalizes in human macrophages in vitro

To determine whether ICG directly binds lipid deposits, as suggested by our histological results, we loaded solutions of ICG alone (100 μM), human acetylated LDL (acLDL) alone (2 mg/ml), and a preincubated combination of ICG (100 μM) and human acLDL (2 mg/ml) onto size exclusion resin columns. Compared to ICG and acLDL alone, preincubation of acLDL and ICG produced a greater peak absorption in fraction 2 (~200 μl; high–molecular weight species), consistent with binding of ICG to acLDL (Fig. 5A). Notably, acLDL alone showed scant absorption at 750 nm, demonstrating that ICG was the main source of the 750-nm signal in the acLDL-ICG group. There was also little signal from ICG alone within fraction 2, given the smaller size of ICG. At the later elution volumes of ~800 μl (lower–molecular weight species), a signal was noted in the ICG-alone group, but with smaller peak values than in fraction 2, presumably due to interactions of ICG with the hydrophobic resin.

Macrophages can ingest albumin, and ICG can bind to albumin (*10*); therefore, we performed a size exclusion column study of ICG (100 μM), bovine serum albumin (BSA; 1 mg/ml), and a preincubated combination of ICG and BSA. Similar to the ICG-acLDL results, the preincubated ICG-BSA combination generated a strong optical absorption in elution fraction 2 that was absent in the BSA-alone group (Fig. 5B). This finding suggests that macrophage

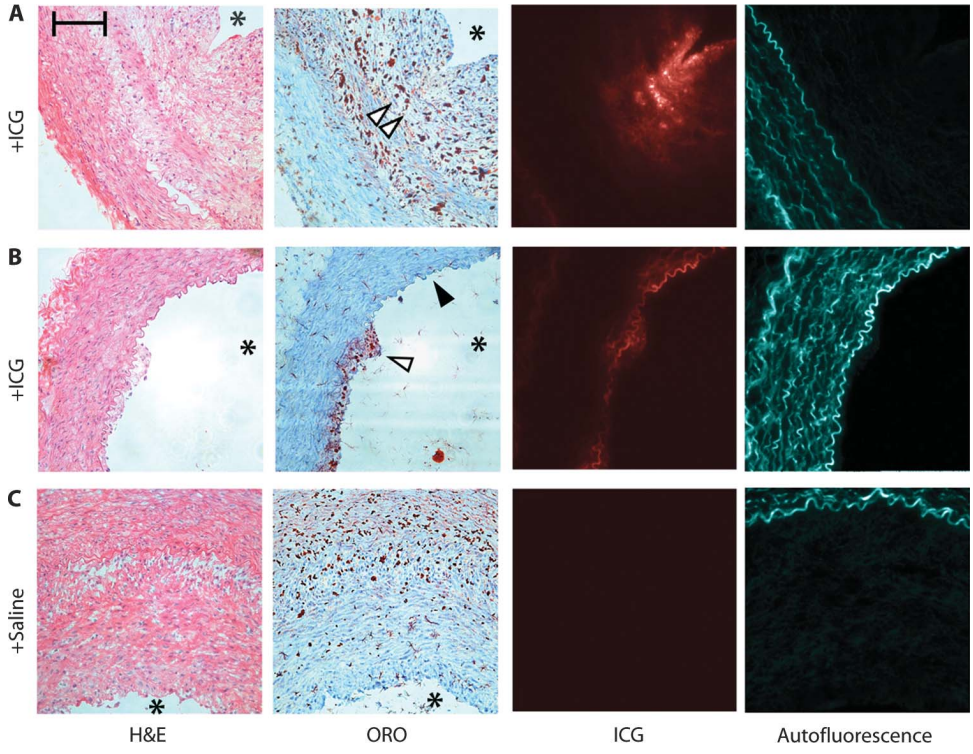

Fig. 3. ICG deposition profile and autofluorescence in various-sized rabbit atheroma. From left to right: hematoxylin-eosin (H&E), for general morphology; ORO; 845-nm fluorescence channel for ICG (false-colored red); and 535-nm channel for autofluorescence from the medial elastic laminae (false-colored blue). Within each group, all images are from adjacent sections (6 μm). (**A**) ICG colocalizes with ORO-positive areas (open arrowheads) in a large atheroma section. (**B**) In a section from a small atheroma, ICG colocalizes with ORO (open arrowhead) and also generates a signal in the superficial intima media in ORO-negative areas (solid arrowhead). (**C**) In saline-injected animals, minimal NIRF signal is evident, but 535-nm channel autofluorescence remains. Asterisks denote the lumen. Scale bar, 100 μm.

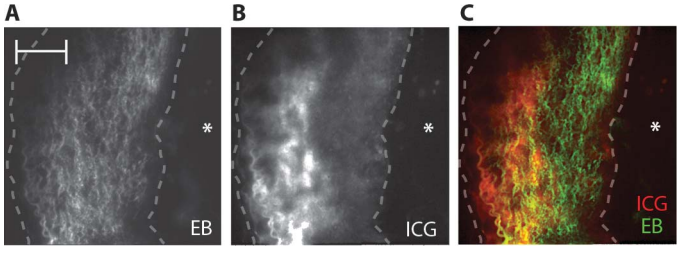

Fig. 4. ICG atheroma-targeting profile in comparison to the Evans blue vascular permeability agent. (**A**) Fluorescence microscopy of Evans blue (EB) (710 nm) demonstrates homogenous signal enhancement in atheroma areas, indicating an impaired endothelial barrier. (**B**) ICG NIRF signal (845 nm) from the same section demonstrates focal signal in the deeper intimal plaque area. (**C**) A fusion image further illustrates the difference between ICG (red) and EB (green) localization in an atheroma. Asterisks denote the location of the lumen. Dashed lines outline atheroma. Scale bar, 100 μm.

uptake of ICG in vivo might occur by phagocytosis of ICG-albumin complexes.

To investigate ICG uptake by macrophages, we incubated human monocyte–derived macrophages (a subset of which was preloaded with acLDL to form foam cells) with or without ICG (25 or 125 μM). Fluorescence microscopy (810 nm) of foam cells incubated with ICG revealed strong NIR fluorescence, in contrast to control foam cells that showed negligible NIR autofluorescence (Fig. 5C). Macrophages incubated for 1 hour with ICG demonstrated concentration-dependent fluorescence at 790 nm. acLDL-induced foam cells showed higher ICG uptake than macrophages (Fig. 5D) in a concentration-dependent manner (Fig. 5E).

ICG enables rapid in vivo detection of lipid-rich, inflamed plaques

To determine whether ICG could provide suitable SNR for in vivo detection of atherosclerosis, cholesterol-fed, balloon-injured rabbits (n = 5) underwent intravascular sensing using a coronary artery guidewire modified to detect NIR fluorescence (figs. S1 and S2). Nonuniform pullback was a limitation of our previous in vivo spectroscopic study (*5*). Hence, to allow uniform pullback in four of the five rabbits, the back end of the fiber was attached to an automated mechanism with a pullback rate of 0.5 mm/s. Rabbits underwent both x-ray angiography (Fig. 6A) and intravascular ultrasound (IVUS) (Fig. 6B) to enable precise co-registration of NIRF signals with x-ray– and IVUS-defined atheroma. After the intravascular NIRF guidewire was placed, baseline NIRF automated pullbacks across aortic atheroma (before ICG injection) revealed minimal NIRF signal (as in Fig. 7B), consistent with low autofluorescence and low electronic noise. ICG was then injected, and serial, dynamic NIRF guidewire pullbacks were performed under x-ray guidance. After 10 to 15 min, to permit ICG washout from the blood pool, the focal NIRF signal evolved and colocalized with atheroma that had been co-registered by x-ray angiography and IVUS images (Fig. 6C). The ex vivo fluorescence reflectance image (FRI) (Fig. 6D) and fusion NIRF-WL image (Fig. 6E) demonstrated a strong NIRF signal in aortic and iliac plaques, corroborating the in vivo NIRF pullback data.

The in vivo peak plaque TBR in ICG-injected animals (n = 5) was 10.3 ± 6.2 (Fig. 7A), which was significantly greater than the baseline plaque TBR before injection (1.4 ± 0.2; $P < 0.05$). NIRF signal profiles before ICG injection showed minimal autofluorescence signal (Fig. 7B, lower left). Analysis of the signals obtained during the serial NIRF guidewire pullbacks revealed that the initial peak arterial signal correlated with saturating blood concentrations of ICG and decayed exponentially over time (Fig. 7B). About 15 to 20 min after injection, however, the peak ICG signal in the vessel localized to atheroma, indicating selective, focal retention of ICG in the plaques. The plaque TBR remained stable during the guidewire sampling period of 20 min until rabbits were killed at 45 min (Fig. 7C), demonstrating that ICG provided durable NIRF plaque enhancement over this time period.

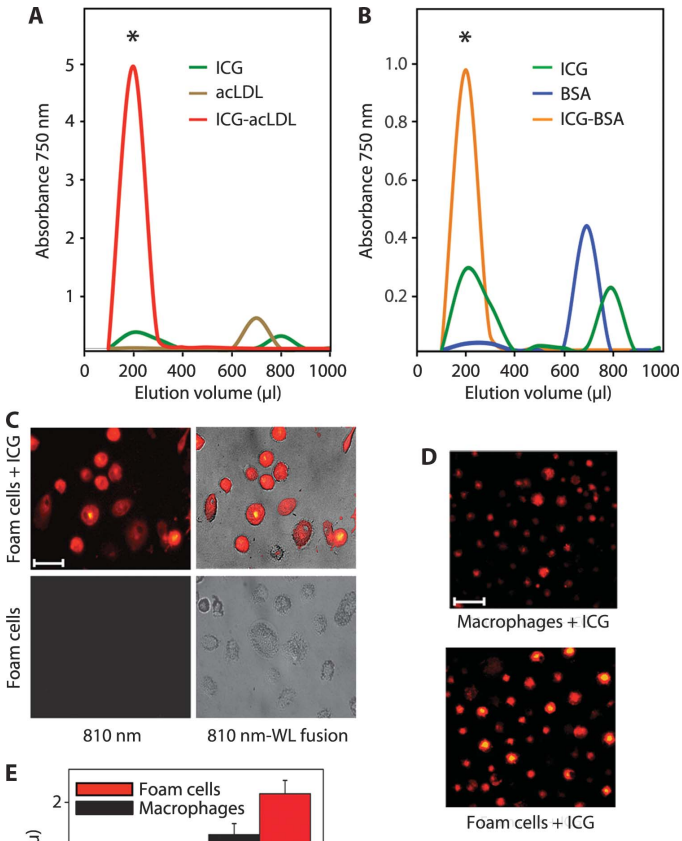

Fig. 5. ICG binding to acetylated LDL and BSA, and uptake by human macrophages. (**A** and **B**) Size exclusion chromatography with optical absorbance measured at 750 nm for serial elutions. Early elutions (*) consisted of higher–molecular weight compounds. (A) Elution profiles of ICG, acetylated LDL (acLDL), and the preincubated ICG-acLDL combination. (B) Elution profiles of ICG, BSA, and the preincubated ICG-BSA combination. (**C**) Fluorescence microscopy of intracellular ICG uptake by foam cells (810 nm; fire color lookup table). Overlay of fluorescence with WL images is shown in the right column. Scale bar, 50 μm. (**D**) ICG uptake by human macrophages and foam cells detected at 810 nm. Scale bar, 100 μm. (**E**) Fluorescence measurements (790 nm) of ICG (25 and 125 μM) uptake by human monocyte–derived macrophages and foam cells (average of $n = 2$ experiments). Data are reported as mean ± SD.

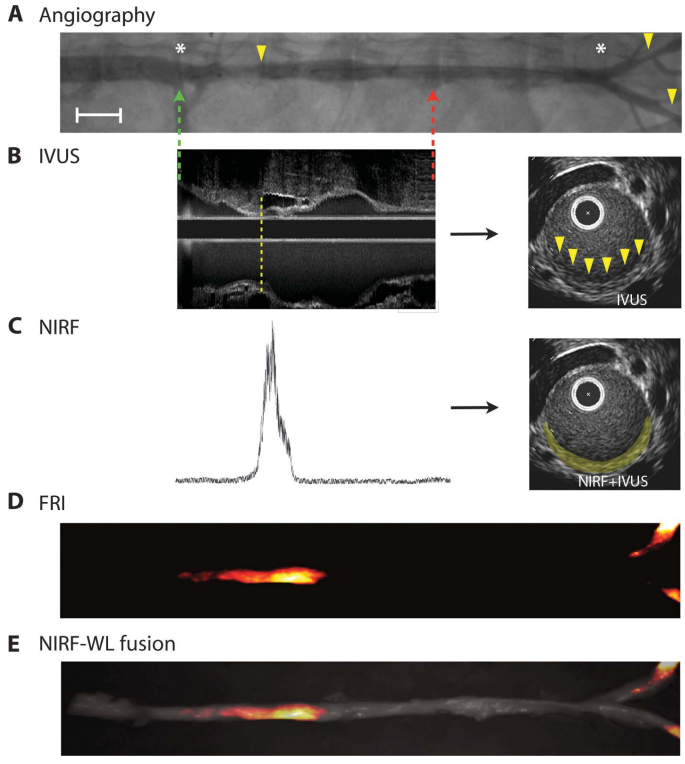

Fig. 6. In vivo intravascular NIRF guidewire sensing of ICG localized in atherosclerotic plaques in rabbits. (**A**) X-ray angiographic images of aortic and iliac luminal narrowings (arrowheads). Green and red dotted arrows represent the start and end of the NIRF guidewire pullbacks, respectively. The white asterisks demarcate arterial branch points. Image was formed by merging two overlapping angiograms. Angiography, in combination with fiducial landmark coordinates from radiopaque tips on both the optical and the IVUS catheters (not shown), allowed for co-registration of the NIRF and IVUS data sets. Scale bar, 1 cm. (**B**) IVUS longitudinal image obtained from an aortic, atheroma-bearing animal (left). A small plaque (intimal thickening) is evident at the lower edge of the dotted yellow line, as seen further on the corresponding axial image on the right (arrowheads). (**C**) Fifteen minutes after ICG injection, a NIRF guidewire signal trace was recorded at 780 nm during automated pullback (left). The NIRF signal (right; false-colored yellow) was fused onto the IVUS-demarcated atheroma in the axial slice shown in (B). All longitudinal images were scaled on the same unit length and matched on the same fiducial markers. (**D**) Ex vivo FRIs show enhanced ICG signal in aortic and iliac plaques (fire color lookup table). (**E**) Overlay of NIRF reflectance image with the white light (WL) image.

To examine the capability of ICG to target and enhance human atheroma, we incubated ICG with freshly resected human carotid endarterectomy specimens at 37°C ($n = 4$ patients). NIR fluorescence microscopy and correlative histological evaluation revealed that ICG colocalized with human plaque macrophages, as evidenced by a fluorescent overlap with $CD68^+$ staining (fig. S3). ICG also colocalized with lipid-rich (ORO-positive) areas, although visually less so than macrophages. ICG did not specifically target collagen in human atheroma, as shown by lack of overlap with Masson's trichrome staining of collagenous areas (fig. S3), and as corroborated by the in vivo ICG atheroma results in rabbits (Fig. 2A). We also noted NIRF signal present at the borders of the specimen, which reflects an edge artifact (fig. S3). As opposed to intravenous injection of ICG in the rabbit study, where ICG may access the plaque interior via penetrating vasa vasorum, ex vivo binding of ICG to plaque components is likely to be diffusion-limited, which results in greater ICG access to the plaque edges compared to the interior of the plaque.

DISCUSSION

Methods are needed to detect coronary arterial plaques that are at risk for rupture. Clinically approved atherosclerosis-targeted contrast agents could enable high-resolution clinical molecular imaging of coronary arterial pathology. Here, we have demonstrated that ICG, an

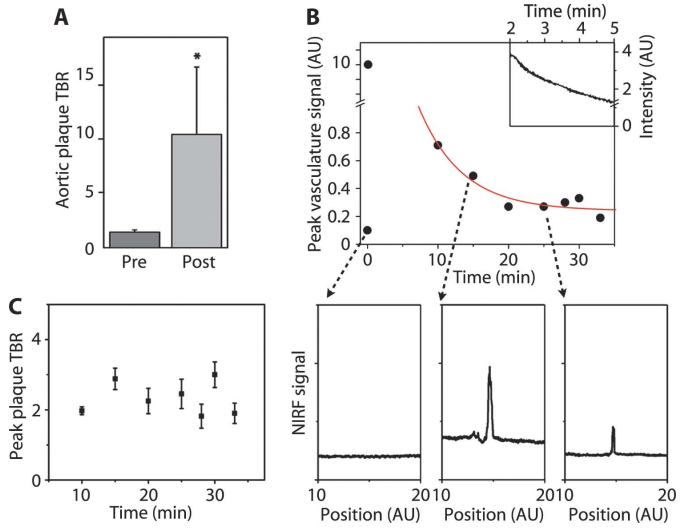

Fig. 7. Focal ICG deposition in rabbit atheroma evolves rapidly after injection and provides stable TBRs. After ICG injection, serial NIRF guidewire pullbacks were performed in vivo through blood, with each pullback initiated distal to plaques and with the starting position confirmed by both IVUS and x-ray angiography. (**A**) The maximum plaque TBR was 10.4 ± 6.2 in the rabbits (n = 5) studied. *P < 0.05 versus the maximum pre–ICG injection TBR (paired t test). (**B**) Immediately after ICG injection, the NIRF guidewire signal recorded a saturating signal [10 arbitrary units (AU)] owing to a high concentration of ICG in the blood, followed by a rapid exponential decay (upper inset). A representative baseline NIRF signal during manual guidewire pullback before ICG injection is shown (below, left). Fifteen minutes (below, middle) and 25 min (below, right) after ICG injection, the NIRF signal presented focal peaks at the site of the atheroma, as visualized on corresponding x-ray angiograms, and registered in real time during x-ray fluoroscopic tracking of the radiopaque NIRF guidewire. Each data point depicts one measurement. The red trendline shows best fit with an exponential decay of the data points from 10 to 33 min. (**C**) Over the course of the imaging session (~45 min), the ICG peak plaque TBR remained stable (n = 5). Error bars show the measurement error of each TBR data point.

FDA-approved NIRF imaging agent, targets lipid- and macrophage-rich atheromas. At clinically approved injection doses (*18*), ICG enables rapid (<20 min) intravascular in vivo detection of lipid-rich, inflamed experimental atheroma in blood-filled arteries of rabbits, similar in caliber (2.5 to 3.5 mm in diameter) to human coronary arteries.

Our histopathological studies of rabbit and human atherosclerosis and in vitro cellular and biochemical analyses have established that the ICG signal reflects several features implicated in atherosclerotic plaque destabilization (*22*), including lipid and macrophage accumulation and possibly endothelial dysfunction, as gauged by heightened vessel permeability (Figs. 2 to 4 and fig. S3). ICG is lipophilic (*10*) and can bind to several plasma lipoproteins, including the atherogenic LDL (*13*). Hence, plaque areas, including foam cell–rich zones, associate closely with ICG deposition (Figs. 2 and 3 and fig. S3). In vitro studies demonstrated that ICG bound to acLDL and to BSA was internalized within human macrophages and foam cells, thus extending previous data (*23*) and shedding new light on mechanisms that might govern ICG accumulation in plaques.

ICG was occasionally deposited in the subendothelial zones of the aortas of cholesterol-fed animals, even when atherosclerosis was not detected by ORO staining (Fig. 3B). Arteries of cholesterol-fed rabbits develop endothelial dysfunction (*24*) and ICG enters the vessel wall in areas of injured endothelium (*25*); in this context, we found that although ICG enters the arterial wall in areas of dysfunctional endothelium and perhaps binds to endothelial cells (*26*), the overall contribution of a permeable endothelium to ICG signal enhancement in vivo appears minor compared to the larger contributions of ICG bound to lipids and macrophages (Figs. 2 and 3 and fig. S3).

We also investigated whether intravascular NIRF technology could be used with ICG to identify lipid-rich, inflamed atheroma in vivo in rabbits, because these features demarcate high-risk plaques responsible for acute myocardial infarction (*27*). The NIRF guidewire enabled sensitive in vivo detection of ICG through blood, with serial pullbacks revealing focal NIRF signal in areas of atheroma, as determined by fiducial co-registered x-ray angiography and IVUS imaging (Fig. 6). The in vivo results provide insights into the kinetics of ICG targeting to atheroma: (i) ICG clears rapidly from the blood, consistent with its short blood half-life of 2 to 4 min after injection (*10*); (ii) within five blood half-lives of ICG elimination (~15 to 20 min), coronary artery–sized plaques become detectable in vivo; (iii) ICG provides durable plaque NIRF signal enhancement with relatively stable TBRs; (iv) detectable NIRF signal in atheroma can be obtained with approved clinical dosages of ICG [1.5 mg/kg bolus, which is below the maximum FDA-approved dose of 2 mg/kg (*18*), especially when allometric scaling is considered (*28*)]; and (v) ICG provides sufficient SNR for detection of enhanced plaques through blood, without the need for balloon occlusion or saline flushing, which attests to the favorable photonic transmission properties of the NIR window (*6*, *7*).

We note that our study has limitations. ICG was not directly investigated in coronary arteries, although the rabbit aorta has a caliber similar to human coronary arteries. Additional mechanistic studies are required to determine whether ICG binds specific lipid components of plaque, such as oxidized LDL, although detection of lipid- or macrophage-rich atheroma demarcates a high-risk plaque subtype (*27*). As demonstrated by correlative fluorescence microscopy and immunohistochemical analyses, not all macrophages exhibited an ICG signal. Further studies analyzing ICG uptake by macrophage subsets (*29*) could prove insightful, but few reagents have been validated for subtyping macrophages in rabbits. For intravascular NIRF detection, we used a one-dimensional spectroscopic sensing fiber that is blind to two-thirds of the vessel circumference (*5*) and is thus subject to sampling bias. New two-dimensional rotational NIRF imaging catheters might overcome this limitation (*30*), provided that sufficient sensitivity can be attained. In addition, we anticipate that integrated single, rather than separate, NIRF and structural imaging catheters [optical coherence tomography (*31*) and IVUS] might enable exact co-registration of NIRF signals with plaques. Additional ICG dosing and timing studies will further optimize the achievable plaque TBR and determine the time duration of detectable ICG signal in plaques. Increased sensitivity could also be obtained by blood displacement via saline flushing, but was not required in this study.

Our findings demonstrate that the FDA-approved agent ICG can provide rapid in vivo biological imaging readouts of lipid- and macrophage-rich plaques in rabbit arteries, through blood-filled vessels, and that ICG targets inflamed, lipid-rich human atheroma specimens ex vivo. The present results offer the possibility of accelerating clinical intracoronary NIRF molecular imaging of atherosclerosis. In addition to providing biological readouts of high-risk plaques, in-

tracoronary detection of plaque ICG could allow examination of the mechanism and efficacy of atherosclerosis therapeutics that alter plaque lipid or macrophages (*32*) and might further elucidate the role of inflammation in provoking coronary stent thrombosis (*33*).

MATERIALS AND METHODS

Animal model and animal preparation

Lipid-rich inflammatory atherosclerosis was induced in New Zealand white rabbits (weight, 3 to 3.5 kg; Charles River Laboratories) by balloon injury of the abdominal aorta and bilateral iliac arteries in combination with an atherogenic diet (*16*, *17*). One week before balloon injury, rabbits consumed a high-cholesterol diet (1% cholesterol and 5% peanut oil, Research Diets Inc.). Rabbits were anesthetized with intramuscular ketamine (35 mg/kg) and xylazine (5 mg/kg) injection. Anesthesia was maintained by mask inhalation of isoflurane [1 to 5% (v/v)] and supplementary oxygen. Arterial balloon injury was performed with a 3F Fogarty arterial embolectomy catheter (Edwards Lifesciences). The catheter was advanced in a 4F sheath (Cordis) into the artery through the right common carotid artery, the balloon was inflated to tension (0.2 to 0.6 ml), and a total of three pullbacks were performed. The introducer was then removed, and the carotid artery was ligated. We used x-ray guidance during the procedure (Siemens). Rabbits continued on a supplemental high-cholesterol diet for 8 more weeks.

We therefore investigated 19 atherosclerotic animals (17 injected with ICG, 2 injected with saline). ICG (Akorn) was injected at a dose of 1.5 mg/kg for in vivo studies. Of the 17 ICG-injected rabbits, 5 were used for in vivo studies and 3 others were co-injected with Evans blue (6 ml of 0.5% solution, Sigma) (*34*). We also used normal New Zealand white rabbits injected with ICG (1.5 mg/kg, $n = 2$). The total number of rabbits used in the study was 21. The Subcommittee on Research Animal Care at Massachusetts General Hospital approved this experimental protocol for all procedures.

Fluorescence reflectance imaging

After the rabbits were euthanized, the arterial tree was perfused with saline and dissected, and connective tissue was removed carefully. The macroscopic fluorescence distribution of ICG in resected vessels was mapped with a commercial FRI system (for atherosclerotic rabbits, $n = 19$, BonSAI system, Siemens; for normal rabbits, $n = 2$, Small Animal Imaging System OV110, Olympus) equipped with an excitation band-pass filter of 716 to 756 nm and an emission band-pass filter of 780 to 820 nm (Omega Optical). WL and ICG fluorescence images were obtained with integration times of 100 ms and 15 s, respectively. Fusion images were created with Matlab software.

Histology

After euthanasia and saline perfusion, arteries underwent immediate FRI and then were fixed in 4% paraformaldehyde for 24 hours. Aortic rings were embedded in optical cutting temperature compound (Sakura Finetek), frozen in chilled isopentane, and sectioned in 6-μm segments. We performed hematoxylin-eosin (H&E) staining for overall plaque morphology, ORO (Sigma) staining to identify lipid-loaded macrophages, Masson's trichrome (Sigma) staining to detect collagen, and van Gieson's (Sigma) staining to show elastin fibers. Adjacent sections were preincubated with 0.3% hydrogen peroxide to inhibit endogenous peroxidase activity and then incubated with primary antibodies: monoclonal mouse anti-human CD31 (clone JC70A; Dako) for endothelial cells, monoclonal mouse anti-human smooth muscle α-actin (clone1A4; Dako), and monoclonal mouse anti-rabbit RAM-11 for macrophages (NeoMarkers). After washing with phosphate-buffered saline (PBS), species-appropriate biotinylated secondary antibodies were applied, followed by avidin-peroxidase complex (Vectastain ABC kit, Vector Laboratories). The reaction was visualized with a 3-amino-9-ethyl-carbazole substrate (DakoCytomation). Sections were counterstained with Harris hematoxylin solution (Sigma) and mounted. Images were captured with a whole-slide microscope scanner (Nanozoomer, Hamamatsu) and with an Eclipse 50i (Nikon) combined with a charge-coupled device (CCD) camera (SPOT RT, Diagnostic Instruments).

Fluorescence microscopy

Fluorescence microscopy was performed with an upright epifluorescence microscope (Eclipse 80i, Nikon) equipped with a cooled CCD camera (Cascade 512B, Photometrics) and an inverted fluorescence microscope (Eclipse TE2000, Nikon) equipped with a CCD camera (Spot Insight QE, Diagnostic Instruments). Images with the epifluorescence microscope were obtained with the following filters: ICG [excitation, 775 ± 25 nm; emission, 845 ± 27 nm; dichroic 810 long pass (LP)], Evans blue (excitation, 650 ± 22 nm; emission, 710 ± 25 nm; dichroic 680 LP), and autofluorescence (excitation, 480 ± 20 nm; emission, 535 ± 25 nm; dichroic 505 LP). ICG images with the inverted fluorescence microscope were acquired with the following filters: excitation, 710 ± 37 nm; emission 810 ± 45 nm; dichroic 750 LP.

All images were analyzed with IP Lab Spectrum software (Scanalytics). Distributions of the ICG fluorescence were determined from images obtained with variable exposure times and subsequently normalized for intensity after noise removal.

In vitro binding of ICG to acLDL

We used a size exclusion resin column (Zeba Spin desalting columns, Pierce) to determine binding. For acLDL binding experiments, samples of 100 μl containing ICG alone (100 μM), human acLDL alone (2 mg/ml), and the preincubated combination of 100 μM ICG and acLDL (2 mg/ml) (37°C for 10 min) were loaded onto columns. For BSA binding experiments, samples of 100 μl containing ICG alone (100 μM), BSA alone (1 mg/ml), and preincubated combination of 50 μM ICG and BSA (1 mg/ml) (37°C for 10 min) were loaded onto similar size-exclusion columns. The columns were then spun at 14,000 rpm for 1 min, and serial elutions of 100-μl aliquots (1000 μl total) were collected using normal saline. Fractions were transferred to a 96-well plate and read by a spectrophotometer with optical density set at 750 nm (SpectraMax Plus, Molecular Devices).

In vitro uptake of ICG by human macrophages

Human peripheral blood monocytes were isolated from freshly prepared leukocyte concentrates by differential centrifugation in Ficoll-Hypaque gradients (*35*). Adherent monocytes differentiated into macrophages over 10 days in culture in RPMI medium containing 5% pooled human serum, L-glutamine, penicillin, and streptomycin (*36*). Macrophage conversion into foam cells was achieved by loading them with acLDL (50 μg/ml) (Biomedical Technologies) for 72 hours. Unloaded macrophages and acLDL-loaded macrophages were incubated with or without ICG (25 and 125 μM) for 60 min. Cells were washed more than three times with PBS. NIR fluorescence (excitation, 730 nm; emission, 790 nm) was measured with a Kodak Digital Science Image Station

4000MM PRO (Eastman Kodak Company, Molecular Imaging Systems). WL and ICG fluorescence images of the cells were then acquired with an inverted fluorescence microscope.

In vivo NIRF guidewire sensing of ICG

The protocol used for the in vivo imaging acquisitions in atheroma-bearing rabbits (n = 5) 8 weeks after balloon injury is illustrated in detail in the flowchart of fig. S1.

X-ray angiography

Aortoiliac x-ray angiography was performed with a manual injection of low-osmolar iodinated contrast agent (5 ml of iopromide, Bayer Healthcare) to image the arterial branches and to determine anatomical landmarks. A radiopaque marker present on the tip of the IVUS catheter combined with the external reference marks (3.8-cm nails) provided the necessary fiduciary points to co-register the NIRF imaging data.

Intravascular ultrasound

IVUS imaging used a 3.2 F monorail catheter with a 40-MHz single-element rotational transducer located proximal to its radiopaque tip and enclosed in an acoustic housing (Boston Scientific). The monorail IVUS catheter was advanced distally into position over a 0.014-inch coronary guidewire. Anatomical landmarks such as the renal vessel branches and the aortoiliac bifurcation were used as reference points. Motorized IVUS pullbacks were performed at 0.5 mm/s. The ultrasound beam resolution was 50 μm in the axial direction and 100 to 200 μm in the lateral direction. To minimize arterial vasospasm, we administered 200 μg of nitroglycerin before intravascular imaging.

Intravascular NIRF sensing apparatus

In vivo ICG data were acquired with a custom-built NIRF guidewire sensing apparatus (fig. S2) (*5*). Excitation light from a continuous wave laser diode at 750 nm is filtered to remove any component present in the ICG fluorescence detection channel. Next, the excitation light is coupled into a 3-dB beam splitter and guided through a fiber for clinical optical coherence tomography (*5*). The guidewire has an outer diameter of 0.41 mm and houses a 62.5/125-μm multimode fiber 200 cm in length. The floppy distal tip of the catheter allows for the fiber to be gently directed through the blood vessels and contains a radiopaque marker for x-ray detection. A prism at the end of the catheter reflects the light at 90° with respect to the catheter axis, focusing the excitation beam on a near diffraction-limited spot size of 40 μm at a working distance of 2 mm. The ICG fluorescence signal is collected in epifluorescence mode through the same optical path used for excitation and guided to a photomultiplier tube (H5783-20, Hamamatsu). Signal is digitized with a 16-bit resolution acquisition card at 1-kHz rate. Data noise reduction and subtraction is performed with Matlab software (MathWorks). The laser power used was <2 mW, as measured by a power meter at the catheter tip.

In vivo spectroscopic sensing of ICG

Rabbits with aortic atherosclerosis (n = 5) underwent intravascular sensing of ICG distribution in vivo. First, the NIRF guidewire was inserted through the carotid artery sheath and percutaneously advanced to the infrarenal aorta. In four of five animals, automated NIRF guidewire pullbacks of 0.5 mm/s were made with the same motorized pullback apparatus as that used for the IVUS imaging system and allowed the fiber to be uniformly scanned axially within the artery. Pullbacks (automated or manual) were made before and then every 5 to 10 min after ICG injection for up to 45 min. Each pullback was initiated far away from the plaque position as determined by both IVUS and x-ray angioscopy, whereas the ICG fluorescence signal was recorded by the photomultiplier and then digitized by a data acquisition card at 1 kHz. X-ray imaging, through the use of fiducial points and in combination with the NIRF guidewire's floppy metal tip, allowed for axial co-registration of both NIRF and IVUS data sets.

Co-registration of NIRF and IVUS images

Care was taken to place fiducial markers (3.8-cm nails) on the rabbit in proximity of the aorta and within the x-ray field of view. The two-dimensional distribution of the fiducial landmarks enabled co-registration of both the IVUS and the optical signal because of the presence of a radiopaque tip on both the optical and the IVUS catheters. Angiography was performed at the time of the stent placement and provided concomitant visualization of the arterial branching. Using the fiduciary coordinates, we matched the automated NIRF signal pullback data to both the angiography images and the IVUS scans before image fusion (Matlab).

Image analysis

FRI data were analyzed with Matlab software. The vessel SNR ratio was obtained as the ratio of the signal calculated on the identified plaque region divided by the noise of the image calculated on proximal areas outside the artery volume. For all analyses, we used similar-sized regions of interest. In addition, we used the WL images to exclude areas with high reflectivity owing to bleed-through–induced artifacts from the emission filters.

Raw FRI data were normalized to the background signal, and the TBR was calculated. We subtracted the calculated background signal to remove camera noise and the optical bleed-through of the reflected light. WL images served to identify atheroma in each aorta that was then thresholded to outline the arterial contour. Vessel areas with excess fat were excluded from TBR and SNR analyses to avoid artifacts because of autofluorescence. Measurements on two regions of interest of similar area and with a length of ~1 cm were performed, with one containing the maximum plaque fluorescence intensity and the other centered in an uninjured area. FRI measurements from two normal rabbits obtained from the BonSAI system were compared to the atherosclerotic FRI measurements by determining the camera noise and subtracting its contribution to calculate TBR and SNR, respectively.

For in vivo NIRF data, NIRF pullbacks were analyzed from the ICG-injected atheroma-bearing rabbits. All the recorded traces were low-pass–filtered, and the maximum intensity was recorded in proximity of the plaque. The maximum signal intensity was always localized in areas of atheroma. The blood background signal was defined as the NIR fluorescence signal measured in the distal part of an uninjured artery. The TBR was then defined as the ratio of the maximum signal intensity to the blood background signal. The measurement variation of the maximum signal and the background signal of each pullback trace were defined as the SD of the noise calculated on the background signal. Error bars on the ratio (TBR) were then determined with the error propagation formula (*37*).

Statistical analysis

Data are presented as mean ± SD. Unpaired and paired Student's t tests were used to assess statistical significance. The one-way analysis

of variance (ANOVA) test followed by a post hoc Tukey's test was also used for multiple comparisons. Values of $P < 0.05$ were considered statistically significant.

SUPPLEMENTARY MATERIAL

www.sciencetranslationalmedicine.org/cgi/content/full/3/84/84ra45/DC1
Methods
Fig. S1. Experimental intravascular NIRF sensing protocol for ICG targeting of atheroma.
Fig. S2. Experimental setup for NIRF spectroscopic sensing.
Fig. S3. Histological sections and fluorescence images of human carotid endarterectomy specimens incubated with ICG.

REFERENCES AND NOTES

1. J. Sanz, Z. A. Fayad, Imaging of atherosclerotic cardiovascular disease. *Nature* **451**, 953–957 (2008).
2. F. A. Jaffer, P. Libby, R. Weissleder, Molecular imaging of cardiovascular disease. *Circulation* **116**, 1052–1061 (2007).
3. R. Virmani, A. P. Burke, F. D. Kolodgie, A. Farb, Vulnerable plaque: The pathology of unstable coronary lesions. *J. Interv. Cardiol.* **15**, 439–446 (2002).
4. B. D. MacNeill, H. C. Lowe, M. Takano, V. Fuster, I. K. Jang, Intravascular modalities for detection of vulnerable plaque: Current status. *Arterioscler. Thromb. Vasc. Biol.* **23**, 1333–1342 (2003).
5. F. A. Jaffer, C. Vinegoni, M. C. John, E. Aikawa, H. K. Gold, A. V. Finn, V. Ntziachristos, P. Libby, R. Weissleder, Real-time catheter molecular sensing of inflammation in proteolytically active atherosclerosis. *Circulation* **118**, 1802–1809 (2008).
6. F. A. Jaffer, P. Libby, R. Weissleder, Optical and multimodality molecular imaging: Insights into atherosclerosis. *Arterioscler. Thromb. Vasc. Biol.* **29**, 1017–1024 (2009).
7. M. A. Calfon, C. Vinegoni, V. Ntziachristos, F. A. Jaffer, Intravascular near-infrared fluorescence molecular imaging of atherosclerosis: Toward coronary arterial visualization of biologically high-risk plaques. *J. Biomed. Opt.* **15**, 011107 (2010).
8. I. J. Fox, L. G. Brooker, D. W. Heseltine, H. E. Essex, E. H. Wood, A tricarbocyanine dye for continuous recording of dilution curves in whole blood independent of variations in blood oxygen saturation. *Proc. Staff Meet. Mayo Clin.* **32**, 478–484 (1957).
9. J. Caesar, S. Shaldon, L. Chiandussi, L. Guevara, S. Sherlock, The use of indocyanine green in the measurement of hepatic blood flow and as a test of hepatic function. *Clin. Sci.* **21**, 43–57 (1961).
10. T. Desmettre, J. M. Devoisselle, S. Mordon, Fluorescence properties and metabolic features of indocyanine green (ICG) as related to angiography. *Surv. Ophthalmol.* **45**, 15–27 (2000).
11. R. W. Flower, Evolution of indocyanine green dye choroidal angiography. *Opt. Eng.* **34**, 727–736 (1995).
12. R. C. Benson, H. A. Kues, Fluorescence properties of indocyanine green as related to angiography. *Phys. Med. Biol.* **23**, 159–163 (1978).
13. S. Yoneya, T. Saito, Y. Komatsu, I. Koyama, K. Takahashi, J. Duvoll-Young, Binding properties of indocyanine green in human blood. *Invest. Ophthalmol. Vis. Sci.* **39**, 1286–1290 (1998).
14. C. P. Herbort, B. Bodaghi, P. Lehoang, Indocyanine green angiography in ocular inflammatory diseases: Principles, schematic interpretation, semiology and clinical value. *J. Fr. Ophtalmol.* **24**, 423–447 (2001).
15. T. Fischer, I. Gemeinhardt, S. Wagner, D. V. Stieglitz, J. Schnorr, K. G. Hermann, B. Ebert, D. Petzelt, R. Macdonald, K. Licha, M. Schirner, V. Krenn, T. Kamradt, M. Taupitz, Assessment of unspecific near-infrared dyes in laser-induced fluorescence imaging of experimental arthritis. *Acad. Radiol.* **13**, 4–13 (2006).
16. Z. S. Galis, G. K. Sukhova, R. Kranzhöfer, S. Clark, P. Libby, Macrophage foam cells from experimental atheroma constitutively produce matrix-degrading proteinases. *Proc. Natl. Acad. Sci. U.S.A.* **92**, 402–406 (1995).
17. M. Aikawa, E. Rabkin, Y. Okada, S. J. Voglic, S. K. Clinton, C. E. Brinckerhoff, G. K. Sukhova, P. Libby, Lipid lowering by diet reduces matrix metalloproteinase activity and increases collagen content of rabbit atheroma: A potential mechanism of lesion stabilization. *Circulation* **97**, 2433–2444 (1998).
18. Akorn, Indocyanine green for injection, USP (2008).
19. G. P. van Nieuw Amerongen, M. A. Vermeer, P. Nègre-Aminou, J. Lankelma, J. J. Emeis, V. W. van Hinsbergh, Simvastatin improves disturbed endothelial barrier function. *Circulation* **102**, 2803–2809 (2000).
20. J. Hed, C. Dahlgren, I. Rundquist, A simple fluorescence technique to stain the plasma membrane of human neutrophils. *Histochemistry* **79**, 105–110 (1983).
21. W. E. Stehbens, Endothelial permeability in experimental aneurysms and arteriovenous fistulas in rabbits as demonstrated by the uptake of Evans blue. *Atherosclerosis* **30**, 343–349 (1978).
22. P. Libby, Inflammation in atherosclerosis. *Nature* **420**, 868–874 (2002).
23. J. M. Rhodes, I. Lind, Antigen uptake in vivo by peritoneal macrophages from normal mice, and those undergoing primary or secondary responses. *Immunology* **14**, 511–525 (1968).
24. T. J. Verbeuren, F. H. Jordaens, L. L. Zonnekeyn, C. E. Van Hove, M. C. Coene, A. G. Herman, Effect of hypercholesterolemia on vascular reactivity in the rabbit. I. Endothelium-dependent and endothelium-independent contractions and relaxations in isolated arteries of control and hypercholesterolemic rabbits. *Circ. Res.* **58**, 552–564 (1986).
25. D. E. Kim, D. Schellingerhout, F. A. Jaffer, R. Weissleder, C. H. Tung, Near-infrared fluorescent imaging of cerebral thrombi and blood–brain barrier disruption in a mouse model of cerebral venous sinus thrombosis. *J. Cereb. Blood Flow Metab.* **25**, 226–233 (2005).
26. R. W. Flower, Binding and extravasation of indocyanine green dye. *Retina* **14**, 283–284 (1994).
27. M. Naghavi, P. Libby, E. Falk, S. W. Casscells, S. Litovsky, J. Rumberger, J. J. Badimon, C. Stefanadis, P. Moreno, G. Pasterkamp, Z. Fayad, P. H. Stone, S. Waxman, P. Raggi, M. Madjid, A. Zarrabi, A. Burke, C. Yuan, P. J. Fitzgerald, D. S. Siscovick, C. L. de Korte, M. Aikawa, K. E. Juhani Airaksinen, G. Assmann, C. R. Becker, J. H. Chesebro, A. Farb, Z. S. Galis, C. Jackson, I. K. Jang, W. Koenig, R. A. Lodder, K. March, J. Demirovic, M. Navab, S. G. Priori, M. D. Rekhter, R. Bahr, S. M. Grundy, R. Mehran, A. Colombo, E. Boerwinkle, C. Ballantyne, W. Insull Jr., R. S. Schwartz, R. Vogel, P. W. Serruys, G. K. Hansson, D. P. Faxon, S. Kaul, H. Drexler, P. Greenland, J. E. Muller, R. Virmani, P. M. Ridker, D. P. Zipes, P. K. Shah, J. T. Willerson, From vulnerable plaque to vulnerable patient: A call for new definitions and risk assessment strategies: Part I. *Circulation* **108**, 1664–1672 (2003).
28. V. Sharma, J. H. McNeill, To scale or not to scale: The principles of dose extrapolation. *Br. J. Pharmacol.* **157**, 907–921 (2009).
29. A. Mantovani, C. Garlanda, M. Locati, Macrophage diversity and polarization in atherosclerosis: A question of balance. *Arterioscler. Thromb. Vasc. Biol.* **29**, 1419–1423 (2009).
30. R. N. Razansky, A. Rosenthal, G. Mallas, D. Razansky, F. A. Jaffer, V. Ntziachristos, Near-infrared fluorescence catheter system for two-dimensional intravascular imaging in vivo. *Opt. Express* **18**, 11372–11381 (2010).
31. D. Stamper, N. J. Weissman, M. Brezinski, Plaque characterization with optical coherence tomography. *J. Am. Coll. Cardiol.* **47**, C69–C79 (2006).
32. D. J. Rader, A. Daugherty, Translating molecular discoveries into new therapies for atherosclerosis. *Nature* **451**, 904–913 (2008).
33. T. F. Lüscher, J. Steffel, F. R. Eberli, M. Joner, G. Nakazawa, F. C. Tanner, R. Virmani, Drug-eluting stent and coronary thrombosis: Biological mechanisms and clinical implications. *Circulation* **115**, 1051–1058 (2007).
34. T. Asahara, D. Chen, Y. Tsurumi, M. Kearney, S. Rossow, J. Passeri, J. F. Symes, J. M. Isner, Accelerated restitution of endothelial integrity and endothelium-dependent function after phVEGF$_{165}$ gene transfer. *Circulation* **94**, 3291–3302 (1996).
35. A. Böyum, Isolation of mononuclear cells and granulocytes from human blood. Isolation of monuclear cells by one centrifugation, and of granulocytes by combining centrifugation and sedimentation at 1 g. *Scand. J. Clin. Lab. Invest. Suppl.* **97**, 77–89 (1968).
36. K. Isoda, E. Folco, M. R. Marwali, F. Ohsuzu, P. Libby, Glycated LDL increases monocyte CC chemokine receptor 2 expression and monocyte chemoattractant protein-1-mediated chemotaxis. *Atherosclerosis* **198**, 307–312 (2008).
37. J. R. Taylor, *An Introduction to Error Analysis* (University Science Books, Sausalito, CA, 1996).

38. **Acknowledgments:** We thank A. Mauskapf, J. L. Guerrero, and M. C. John for rabbit surgical studies; G. Mallas for assistance with intravascular NIRF signal detection; G. Sukhova for histology and staining of human carotid endarterectomy samples; and P. Fumene Feruglio and T. Quillard for assistance in image processing. **Funding:** NIH R01 HL108229 (F.A.J.), American Heart Association Scientist Development Grant #0830352N (F.A.J.), Howard Hughes Medical Institute Career Development Award (F.A.J.), and Donald W. Reynolds Foundation (E.A., R.W., P.L., and F.A.J.). C.V. acknowledges support from NIH RO1-EB006432, PO1-AI054904. **Author contributions:** F.A.J. conceived the study, assisted in data analysis, acquired experimental rabbit data, and supervised the project. C.V. and F.A.J. wrote the manuscript. C.V. generated the in vivo imaging measurements and analyzed the data. I.B. led the surgical procedures, performed the IVUS and angiography measurements, and analyzed the microscopy and FRI data. E.A. and Y.I. performed histopathological analyses. M.A.C. and E.J.F. performed and analyzed the in vitro ICG uptake and binding studies and contributed to writing the paper. P.L., R.W., and V.N. assisted with experimental design and contributed to writing the paper. **Competing interests:** F.A.J. has received a patent for ICG detection of atherosclerosis that has been assigned to Massachusetts General Hospital (F. A. Jaffer, Detection of atherosclerosis using indocyanine green. United States Patent Application 20100092389).

Submitted 10 August 2010
Accepted 6 May 2011
Published 25 May 2011
10.1126/scitranslmed.3001577

Citation: C. Vinegoni, I. Botnaru, E. Aikawa, M. A. Calfon, Y. Iwamoto, E. J. Folco, V. Ntziachristos, R. Weissleder, P. Libby, F. A. Jaffer, Indocyanine green enables near-infrared fluorescence imaging of lipid-rich, inflamed atherosclerotic plaques. *Sci. Transl. Med.* **3**, 84ra45 (2011).